2022-06

Assessment of equivalent substrate stiffness and mechanical properties of sustainable alkali-activated concrete containing recycled concrete aggregate

Damrongwiriyanupap, N

10.1016/j.cscm.2022.e00982
Case Studies in Construction Materials
Elsevier

Case Studies in Construction Materials 16 (2022) e00982

Contents lists available at ScienceDirect

Case Studies in Construction Materials

journal homepage: www.elsevier.com/locate/cscm

Assessment of equivalent substrate stiffness and mechanical properties of sustainable alkali-activated concrete containing recycled concrete aggregate

Nattapong Damrongwiriyanupap [a], Todsaporn Srikhamma [b], Chittinat Plongkrathok [b], Tanakorn Phoo-ngernkham [b,*], Worathep Sae-Long [a], Sakonwan Hanjitsuwan [c], Piti Sukontasukkul [d], Long-yuan Li [e], Prinya Chindaprasirt [f,g]

[a] Department of Civil Engineering, School of Engineering, University of Phayao, Phayao 56000, Thailand
[b] Sustainable Construction Material Technology Research Unit, Department of Civil Engineering, Faculty of Engineering and Technology, Rajamangala University of Technology Isan, Nakhon Ratchasima 30000, Thailand
[c] Program of Civil Technology, Faculty of Industrial Technology, Lampang Rajabhat University, Lampang 52100, Thailand
[d] Construction and Building Materials Research Center, Department of Civil Engineering, Faculty of Engineering, King Mongkut's University of Technology-North Bangkok, Bangkok 10800, Thailand
[e] School of Engineering, Faculty of Science and Engineering, Plymouth University, PL4 8AA, United Kingdom
[f] Sustainable Infrastructure Research and Development Center, Dept. of Civil Engineering, Faculty of Engineering, Khon Kaen University, Khon Kaen 40002, Thailand
[g] Academy of Science, The Royal Society of Thailand, Dusit, Bangkok 10300, Thailand

ARTICLE INFO

Keywords:
Sustainable alkali-activated concrete
Equivalent substrate stiffness
Mechanical properties
Recycled concrete aggregate
Life-cycle assessment

ABSTRACT

The effects of using recycled concrete aggregate (RCA) as coarse aggregate on the equivalent substrate stiffness and mechanical properties of sustainable alkali-activated concrete were investigated in this paper. High-calcium fly ash (HFA) and commercial silica fume (SF) were used as the precursors for producing the alkali-activated high-calcium fly ash concrete (AAHFAC). Sodium hydroxide (SH) and sodium silicate (SS) solutions were used as alkaline activator solutions with the constant SS/SH ratio of 1.0 and liquid-binder (L/B) ratio of 0.50. The natural coarse aggregate (NCA) used in this study was crushed limestone and replaced with RCA at the rates of 0%, 20%, 40%, 60%, 80%, and 100% by volume. The setting time, compressive strength, elastic modulus, Poisson's ratio, and bond strength obtained by pull-out tests of AAHFAC and Portland cement concrete (NC) were investigated. Experimental results showed that the use of RCA to replace NCA resulted in reducing the setting time of concrete. Also, the setting time of the AAHFAC with and without SF were shorter than that of NC mixes for all of RCA replacement level. The use of RCA had a positive effect on the mechanical properties of alkali-activated binder; however, they declined at NC mixes. Therefore, the use of RCA in alkali-activated binder concrete is an excellent alternative for sustainable concrete since it allows for the substitution of natural resource components while somehow producing low CO_2 emissions.

* Corresponding author.
E-mail address: tanakorn.ph@rmuti.ac.th (T. Phoo-ngernkham).

https://doi.org/10.1016/j.cscm.2022.e00982
Received 20 December 2021; Received in revised form 20 February 2022; Accepted 23 February 2022
Available online 24 February 2022

1. Introduction

Although ordinary Portland cement (OPC) is a classic construction material widely used as a cementing material for construction works, the manufacturing process emits large amount of carbon dioxide (CO_2) to the atmosphere [1,2]. It is well-known that Portland cement concrete (PCC) simply called normal concrete (NC) consists of OPC, fine and coarse aggregates, and water. However, PCC production consumes large amount of non-renewable natural resources such as sand, gravel, limestone. This causes significant reduction of natural resources which must be considered seriously. In order to solve this problem, several researchers [3–5] attempted to utilize waste from construction and demolition sites such as old building concrete, defective precast concrete, concrete block, reclaimed asphalt pavement, and so on, as an alternated aggregate source. These wastes from construction and demolition sites, if not being utilized, are mostly ended up in landfills.

There are many types of recycled aggregate (RA), which can be used to replace natural aggregates (NA) (sand and limestone) in concrete manufacturing. Wongsa et al. [5] claimed that the RA from different areas can be used to fabricate Portland cement composites. However, some researchers [5–7] demonstrated that the mechanical properties of concrete are strongly affected by the properties of RAs. This is due to the weakness and high porosity of RAs as compared to crushed natural limestone, which leads to poor quality concrete [6]. Nowadays, recycled concrete aggregate (RCA) with a compressive strength of about 35–50 MPa has been widely studied in producing concrete, as reported by Arabiyat et al. [8]. They reported that RCA with relatively high strength could be used to replace the natural coarse aggregate (NCA). Many studies were conducted on utilizing RCA in concrete. For instance, RCA was applied to replace NCA to investigate the shear behavior of concrete beams [8]. Their results showed that the shear capacity increased as the RCA replacement level increased. Nobre et al. [6] developed a novel dry-mix shotcrete combined with coarse RCA. In general, the performance of shotcretes mixed with RCA is not so good as those mixed with NCA due to the higher water absorption of coarse RCA.

Green material called "alkali-activated binder" has been developed by several researchers [5,9–16] to use as an alternative material for cement and concrete. Alkali-activated binder (AAB) can be synthesized by the chemical reactions between aluminosilicate materials and alkaline solutions [17–21]. In Thailand, the fly ash (FA) from Mae Moh power plant has been used as the precursor for AAB because of its vast availability and suitable chemical compositions (i.e., SiO_2, Al_2O_3, and CaO). From Chindaprasirt et al. [22] study, it was demonstrated that the coexistence of SiO_2 and CaO in the AAB matrix helped the geopolymerization process to occur at ambient temperature, which made it an ideal material for repairing works. Phoo-ngernkham et al. [11,23–25] carried out a pioneering work on a novel sustainable repair material made from alkali-activated high-calcium FA. It was found suitable as an alternative repair material with advantages on environmental friendliness and cost effectiveness. For the utilization of RCA in AAB concrete, a number of researchers [5,12,26–28] examined the possibility of using RCA as fine and/or coarse aggregates. For example, Wongsa et al. [5] applied RCA in pressed FA geopolymer in the production of masonry block. They concluded that geopolymer concrete block containing RCA can be used to produce hollow blocks with excellent insulating properties. Pasupathy et al. [28] also studied the thermal insulation properties of aerated geopolymer foam concrete incorporated with RCA. The results showed that using RCA in aerated geopolymer foam concrete improved the thermal conductivity. In addition, Rahman et al. [12] studied the mechanical properties of roller-compacted geopolymer concrete and roller-compacted cement concrete using 100%RCA as a coarse aggregate. It was found that the mechanical properties of roller-compacted geopolymer concrete were similar to roller-compacted cement concrete. Moreover, some researchers [3,29,30] studied the stress-strain relationship of low-calcium based geopolymer concrete and slag based geopolymer concrete incorporated with RCA as a coarse aggregate. They reported that the application of RCA as a coarse aggregate for producing geopolymer concrete led to an increase strain capacity.

According to the above literature review, it could be seen that there are very few studies on the use of RCA in AAHFAC. This paper aims to investigate the effect of RCA on the mechanical properties of AAHFAC. The setting time, compressive strength, modulus of elasticity, Poisson's ratio, and bond strength of the AAHFAC incorporating RCA as a coarse aggregate were examined. The outcomes of this study would add to an existing body of knowledge on the future application of the AAHFAC comprising RCA, especially as an alternate repair material. It should be mentioned that the key weakness of RCA is the part of mortar and the interface transition zone (ITZ) between mortar and aggregate in RCA. However, when the RCA is used in alkali-activated concrete (AAC) the old mortar and old ITZ will be improved significantly by the AAB during the mixing process. Hence, the effect of RCA on the mechanical properties of AAC with RCA would not be so obvious as that in OPC concrete, and in some circumstances the RCA may turn a positive effect on the performance of AAC when it uses the RCA.

2. Experiments and analysis

2.1. Materials

The AAHFAC was made from high-calcium fly ash (HFA) retrieved from Mae Moh power plant in northern Thailand and silica fume (SF); whereas Portland cement is the main precursor for making NC. The HFA had a specific gravity of 2.64 and median particle size of 15.5 micrometer. The average particle sizes of SF was 0.22 μm with specific surface area (BET) of 21,000 m^2/kg. A 10 M sodium hydroxide (SH) solution and sodium silicate (SS) solution with 11.67% Na_2O, 28.66% SiO_2 and 59.67% H_2O were used as liquid activators. Note that the silica modulus (SiO_2/Na_2O molar ratio) was 0.70, whereas total Na_2O+SiO_2 content was 28% by mass of the binder. This low silica modulus was necessary to ensure the workability of AAHFAC. In addition, the superplasticizer (SP) was also added to improve its workability. The chemical compositions of HFA and SF are shown in Table 1, whereas XRD patterns of HFA and SF are illustrated in Fig. 1.

2.2. Aggregate

The natural coarse aggregate (NCA) used in this study was crushed limestone with a maximum size of 9.5 mm. The RCA was obtained from crushing old concrete with compressive strength ranging from 35 to 45 MPa with a maximum size of 9.5 mm. The texture and shape of RCA are shown in Fig. 2. Local river sand (RS) was used as a fine aggregate. The properties of RS, NCA, and RCA are illustrated in Table 2.

2.3. Mixture proportion

Tables 3 and 4 list the mix proportions of the AAHFAC and NC concrete. The mix design approach of the AAHFAC mixes was based on the work represented by Phoo-ngernkham et al. [10]. Both SS/SH ratio of 1.0 and L/B ratio of 0.50 were fixed constantly in the production of AAHFAC mix. A slump of around 200±25 mm was controlled to ensure the workability of AAHFAC [10]. For NC, the mix design was based on ACI211–91 [31] with a target 28-day compressive strength of 28 MPa and slump around 100±25 mm. The RCA was used to replace NCA at the rates of 0%, 20%, 40%, 60%, 80%, and 100% by volume. The moisture content of RS, NCA, and RCA aggregates were controlled at saturated surface dry condition (SSD) for all mixtures.

The production of AAHFAC began with mixing of all aggregates (RS, NCA, and RCA) and SH solution for about 30 s. Then, binder (HFA and HFA with SF) was added and mixed again for 60 s. Right after, SS and SP solutions were added, and the mixing continued for another 60 s

2.4. Testing of specimens

After mixing, the setting times of the AAHFAC and NC were determined in accordance to ASTM C403/C403M-16 [32]. The fresh AAHFAC and NC were cast into cylinder molds with 100 mm diameter and 200 mm height to measure the properties of concrete under uniaxial compression. They were demoulded at the age of 24 h and then immediately wrapped with the vinyl sheet to protect moisture loss and kept in a 25 ºC controlled room for 28 days before the day of test. Determination of elastic modulus and Poisson's ratio of the AAHFAC and NC were carried out as described in ASTM C469 [33]. Three identical samples were tested for each mix and the average value was used as the test result.

The 200 × 200 × 200 mm^3 cube samples with a 12 mm diameter deformed bar were used to determine the pull-out force under a static monotonic load using the ASTM C234 [34] and RILEM method [35]. The bond length of sample was 50 mm as described in RILEM method [35]. To prevent an unexpected transfer of force between the reinforcement and the concrete, the reinforcing bars were encased in plastic tubes [36], as illustrated in Fig. 3. An LVDT was used to determine the sample slip at the end of deformed bar, and a load cell was used to measure the pullout force, and the results were recorded using a data logger. A hydraulic jack was employed to continuously apply load at a rate of 20 kN/min. Fig. 3 illustrates the experimental set-up and conceptualization of the equivalent substrate stiffness (k_s) for pullout test of the AAB and NC. The bond strengths between concrete and reinforcing bar were evaluated at 28 days of curing, and the reported values represent the average of three samples. The following equation is used to calculate the ultimate bond strength:

$$\tau = \frac{F}{\pi l d} \tag{1}$$

Where $\tau$is the ultimate bond stress (MPa), F is the ultimate pullout force (N), $l$is the bond length (mm), and $d$is the diameter of reinforcing bar (mm).

3. Results and discussion

3.1. Setting time

Figs. 4–5 show the results for the setting times of the AAHFAC, whereas the setting times of the NC are illustrated in Fig. 6. It is found that the use of RCA in the AAHFAC and NC decreased the setting time of concrete. According to Figs. 4–6, the initial and final setting times were 18–29 min and 41–63 min for the AAHFAC without SF, 9–20 min and 16–34 min for the AAHFAC with SF, and 161–193 min and 231–263 min for the NC, respectively. The reduction in setting time of both AAHFAC and NC was due to the lower bulk density and water absorption value of RCA [5]. For the effect of RCA on setting time, Wongsa et al. [5] reported that the $Ca(OH)_2$ in the cement mortar on the RCA surface could react with SiO_2 from HFA. This is why the setting time tends to decrease with increased RCA contents.

Table 1
Chemical compositions of FA and SF (wt%).

Materials	SiO_2	Al_2O_3	Fe_2O_3	CaO	MgO	K_2O	Na_2O	SO_3	LOI
HFA	31.33	13.95	15.65	25.78	2.95	2.94	2.84	3.30	1.31
SF	93.30	0.24	–	0.83	0.61	1.50	0.07	0.08	3.18
PC	20.81	4.69	3.40	65.3	1.50	0.40	0.10	2.69	1.0

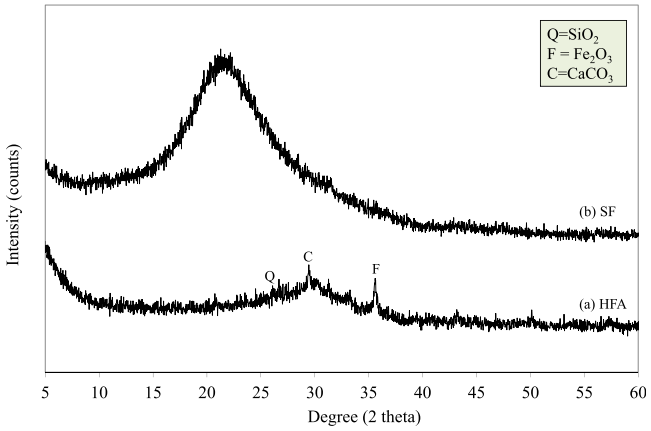

Fig. 1. XRD patterns of HFA and SF.

Fig. 2. RCA after crushed and sieved.

Table 2
Properties of aggregates used in this study.

Types of aggregate	Specific gravity (SG)	Fineness modulus (FM)	Water absorption (%)
Fine aggregate (RS)	2.64	2.42	0.78
Crushed limestone aggregate (NCA)	2.72	6.02	1.71
Recycled concrete aggregate (RCA)	2.39	5.97	8.97

Table 3
Mix proportions of AAHFAC (kg/m^3).

Mix No.	Mix symbol	FA (kg)	SF (kg)	RS (kg)	NCA (kg)	RCA (kg)	SH (kg)	SS (kg)	SP (%)
1	AAHFAC-0RCA	470	–	539	1165	–	117.5	117.5	0.50
2	AAHFAC-20RCA	470	–	508	932	233	117.5	117.5	0.50
3	AAHFAC-40RCA	470	–	477	699	466	117.5	117.5	0.60
4	AAHFAC-60RCA	470	–	445	466	699	117.5	117.5	0.65
5	AAHFAC-80RCA	470	–	414	233	932	117.5	117.5	0.75
6	AAHFAC-100RCA	470	–	383	–	1165	117.5	117.5	0.80
7	AAHFAC-SF-0RCA	423	47	530	1165	–	117.5	117.5	0.55
8	AAHFAC-SF-20RCA	423	47	498	932	233	117.5	117.5	0.55
9	AAHFAC-SF-40RCA	423	47	467	699	466	117.5	117.5	0.65
10	AAHFAC-SF-60RCA	423	47	436	466	699	117.5	117.5	0.70
11	AAHFAC-SF-80RCA	423	47	405	233	932	117.5	117.5	0.85
12	AAHFAC-SF-100RCA	423	47	374	–	1165	117.5	117.5	1.00

Table 4
Mix proportions of NC (kg/m^3).

Mix No.	Mix symbol	PC (kg)	RS (kg)	NCA (kg)	RCA (kg)	Water (kg)	SP (kg)
1	NC-0RCA	410	905	740	–	225	–
2	NC-20RCA	410	885	592	148	225	0.20
3	NC-40RCA	410	865	444	296	225	0.40
4	NC-60RCA	410	845	296	444	225	0.50
5	NC-80RCA	410	826	148	592	225	0.50
6	NC-100RCA	410	806	–	740	225	0.55

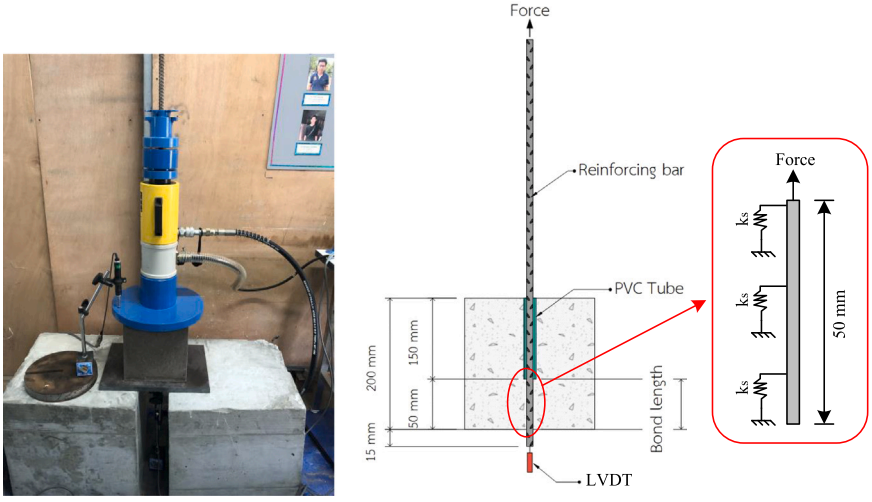

Fig. 3. Experimental set-up and conceptualization of the equivalent substrate stiffness (k_s) for pullout test.

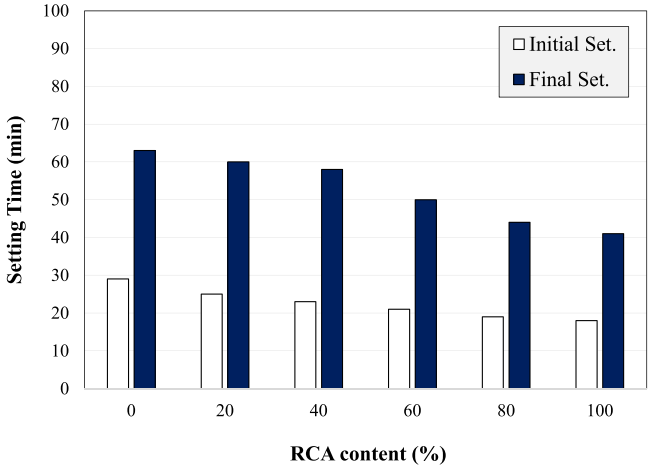

Fig. 4. Setting time of AAHFAC under different RCA contents.

For the effect of SF, the AAHFAC incorporating SF (see Fig. 5) showed faster setting time as compared to the AAHFAC without SF (see Fig. 4). Chindaprasirt et al. [37] reported that the reactive SiO_2 from SF reacted with CaO from HFA and formed additional CSH within the matrix. This agrees with the XRD pattern of the SF, which it is mainly comprised of amorphous phase according to Fig. 1. Hence, the setting time of AAHFAC incorporating SF was much faster than that of the AAHFAC without SF.

3.2. Compressive strength

The increase in the RCA replacement ratio had effects on the compressive strength of both AAHFAC and NC, as illustrated in Fig. 7. According to Fig. 7, the 28-day compressive strengths of AAHFAC and AAHFAC with SF increased with increasing RCA replacement

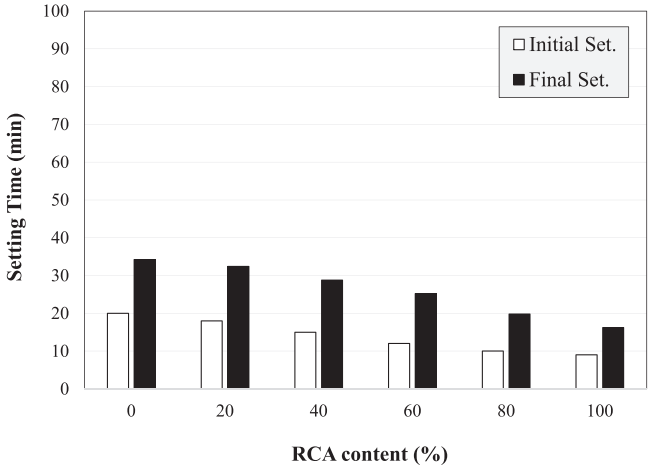

Fig. 5. Setting time of AAHFAC incorporating SF under different RCA contents.

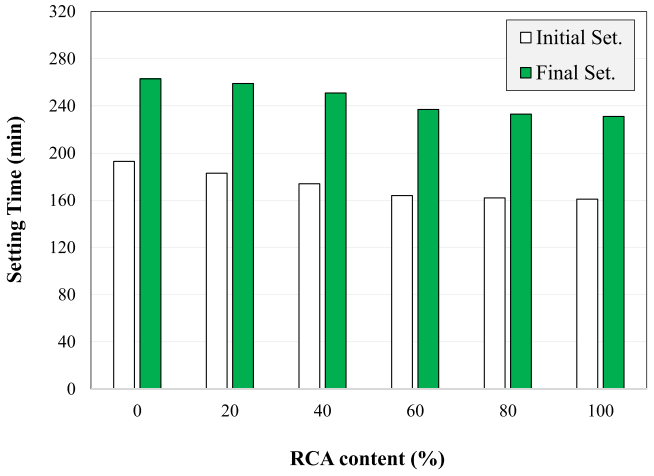

Fig. 6. Setting time of NC under different RCA contents.

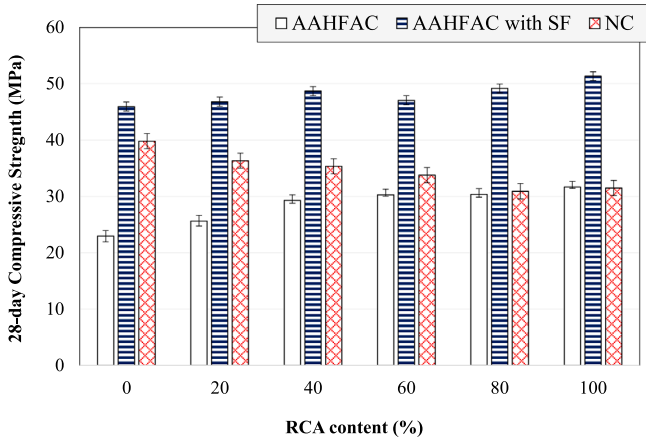

Fig. 7. Compressive strength of AAHFAC, AAHFAC with SF, and NC under different RCA contents.

ratio. They were 23.0–31.7 MPa for the AAHFAC and 46.0–51.3 MPa for AAHFAC with SF. As is observed from Fig. 7, the strength of AAHFAC with SF is higher than that of the AAHFAC. The significant increase in strength development is because the reactive SiO_2 from SF reacted with CaO from HFA (see Fig. 1) to form the formation of C-S-H coexisted with N-A-S-H or geopolymer gel [38,39]. Hanjitsuwan et al. [38] and Phoo-ngernkham et al. [11] demonstrated that the coexistence of C-S-H and N-A-S-H within that matrix contributed to its strength development. Also, the additional formation of C-S-H was obtained from the $Ca(OH)_2$ on the RCA surface [40] reacted with SiO_2 and Al_2O_3 from the precursors and became the pozzolanic reaction products. This also agreed with Li et al. [41] that the strength development of alkali-activated binder tended to increase with increasing CaO content in the mixture. Furthermore, unreacted cement grain existing in RCA during the crushing of old concrete react with water and form hydration products including C-S-H. This is why the strength of the AAHFAC incorporating SF is increased. However, a different trend of strength development for the NC incorporating RCA as a coarse aggregate was observed, as shown in Fig. 7. The reduction in the strength of NC was found as the RCA replacement level increased. Sata et al. [42] reported that the interfacial transition zone in concrete incorporating RCA was weakened. Also, the presence of $Ca(OH)_2$ on the RCA surface in the NC mixes is the negative factor on its strength development. From Kroehong et al. [43] study, it revealed that the existence of $Ca(OH)_2$ in the Portland cement paste produced many chemical reactions in the system, leading to expansion and cracks in concrete. In addition, Rattanachu et al. [40] demonstrated that the high moisture content and high water absorption of RCA induced the water to enter in the RCA despite the RCAs were soaked in water for 24 h to obtain the SSD condition. This may lead to a reduction of W/C ratio within the matrix. It can be noted that using RCA as a coarse aggregate is a good option for producing the AAHFAC. The reaction between $Ca(OH)_2$ on the RCA surface and SiO_2 from the precursors produced high bonding at the interfacial transition zone. Therefore, this is very attractive for using RCA in construction work when alkali-activated concrete is used.

3.3. Stress-strain curves under uniaxial compression

Table 5 and Figs. 8–10 show all of the compressive stress-strain curves of the AAHFAC and NC at the age of 28 days. The measurement of elastic modulus and Poisson's ratio of the samples was conducted as described in ASTM C469 [33]. As illustrated in the Figures, the strain of concrete increased with increased stress of concrete up to the peak stress, followed by a subsequent descending stage. A higher strain was observed when the RCA replacement was increased, as shown in Table 5. According to Figs. 8–10, more deformation behavior of concrete corresponded to a high energy-absorption capacity that is increased the ductility of concrete [44–46]. The elasticity modulus in NC was found to generally increase with the RCA replacement rate, which is consistent with other reported results [47]. However, for AAHFAC and AAHFAC incorporated with SF, the elastic modulus was found to increase if the RCA replacement rate is low, but decrease if the replacement rate is high. Sofi et al. [48] claimed that the stiffness of concrete depended on the strength of paste and aggregates. Also, Tangchirapat et al. [49] reported that the strength of the aggregates was an important factor in the elastic modulus of concrete. This is the main reason why the incorporation of RCA decreased the elastic modulus in the AAHFAC mixes. However, the increased elastic modulus of the AAHFAC mixed with SF was probably due to the $Ca(OH)_2$ on the RCA surface reacted with SiO_2 from HFA and SF as well as the hydration reaction of unreacted cement particle surrounding the surface of RCA. This again could improve the reaction at the contact zone between the RCA surface and the alkali-activated binder. The values of elastic modulus obtained from this study are similar to those reported in the previous studies [10,50,51]. There were between 17 and 25 GPa for alkali-activated concrete and 25 and 35 MPa for conventional concrete. For the results of Poisson's ratio, it is found that the Poisson's ratio for the AAHFAC, AAHFAC with SF, and NC mixes showed a little change with increasing the RCA contents. They were in the range of 0.171–0.221 for the NC mixes, 0.215–0.286 for the AAHFAC mixes; and 0.204–0.232 for the AAHFAC incorporating SF, respectively. The Poisson's ratio values of the NC are consistent with the normal strength of the NC [48]. However, the Poisson's ratio

Table 5
Mechanical parameters of AAHFAC and NC under uniaxial compression.

Mix symbol	$f_c^{'}$ (MPa)	E (GPa)	ε at peak σ_u	υ
AAHFAC-0RCA	23.0	16.3	0.00182	0.236
AAHFAC-20RCA	25.7	17.3	0.00207	0.286
AAHFAC-40RCA	29.3	13.9	0.00268	0.240
AAHFAC-60RCA	30.3	14.5	0.00265	0.255
AAHFAC-80RCA	30.4	14.0	0.00248	0.215
AAHFAC-100RCA	31.7	11.1	0.00320	0.227
AAHFAC-SF-0RCA	46.0	18.3	0.00268	0.225
AAHFAC-SF-20RCA	46.8	20.2	0.00274	0.232
AAHFAC-SF-40RCA	48.7	22.0	0.00289	0.229
AAHFAC-SF-60RCA	47.1	19.5	0.00283	0.219
AAHFAC-SF-80RCA	49.2	18.1	0.00323	0.204
AAHFAC-SF-100RCA	51.4	18.5	0.00339	0.206
NC-0RCA	39.8	29.0	0.00186	0.210
NC-20RCA	36.3	32.2	0.00158	0.193
NC-40RCA	35.3	30.3	0.00181	0.201
NC-60RCA	33.8	31.1	0.00192	0.221
NC-80RCA	30.9	32.9	0.00104	0.213
NC-100RCA	31.5	33.8	0.00123	0.171

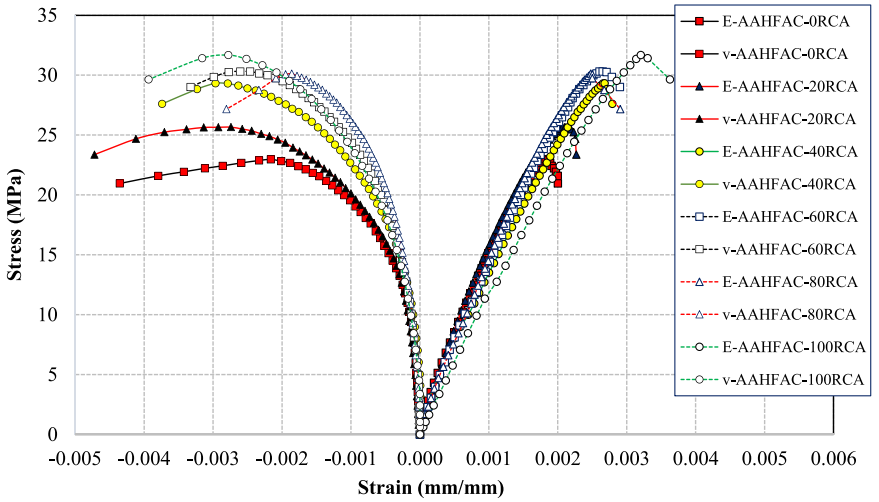

Fig. 8. Compressive stress-strain curves of AAHFAC under different RCA contents.

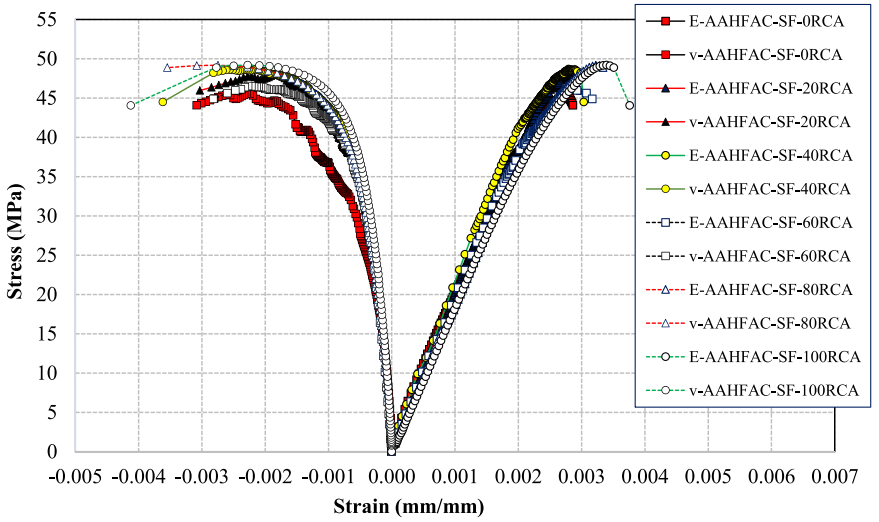

Fig. 9. Compressive stress-strain curves of AAHFAC incorporating SF under different RCA contents.

values of alkali-activated binder exhibited in the same ranges for high-strength concrete, which were between 0.21 and 0.27, as reported by Sofi et al. [48].

3.4. Bond strength of reinforced concrete

Fig. 11 shows the bond strength of all concrete under different RCA contents. In general, the effect of RCA on the bond strength was found to be similar to its effect on the compressive strength of the mixed concrete. The bond strengths of AAHFAC and AAHFAC with SF increased with increasing RCA replacement; however, the bond strength of NC decreased with increasing RCA replacement, which is consistent with the findings of Alhawat and Ashour [52]. For instance, the bond strengths of AAHFAC-0RCA, AAHFAC-60RCA, AAHFAC-SF-0RCA, AAHFAC-SF-60RCA, NC-0RCA, and NC-60RCA were 12.66, 16.70, 24.73, 27.42, 30.58, and 22.55 MPa, respectively. When AAHFAC and AAHFAC with SF are compared, it is observed that the reactive SiO_2 from SF has a substantial effect on bond strength growth than SiO_2 from HFA. This reactive SiO_2 could react with the $Ca(OH)_2$ on the RCA surface and hence the formation of C-(A)-S-H coexisted with N-A-S-H gels [23,53]. Phoo-ngernkham et al. [23] demonstrated that combining C-(A)-S-H and N-A-S-H strengthened the interaction between concrete and AAB. This is why the AAB including RCA has a stronger bond.

The load-slip curves for concrete pullout specimens with deformed bar under different RCA contents are shown in Figs. 12–14. As displayed in Figs. 12–14, the load capacity initially was rather high, with a relatively steep curve; nevertheless, the slope of the curve progressively increased to a peak value. Following that, the bond stress began to drop as the strengthened steel bar began to slip out from surrounding concrete [54,55]. The load-slip relationship for deform bars embedded in AAHFAC and AAHFAC with SF followed

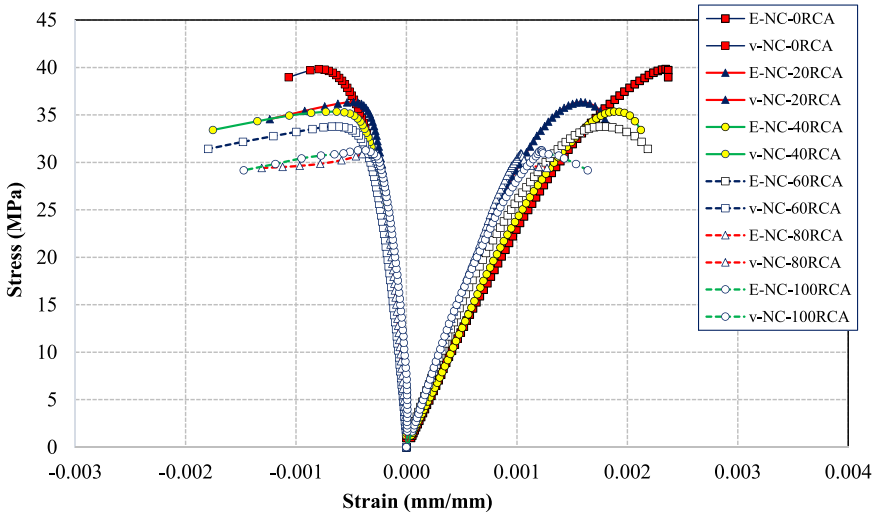

Fig. 10. Compressive stress-strain curves of NC under different RCA contents.

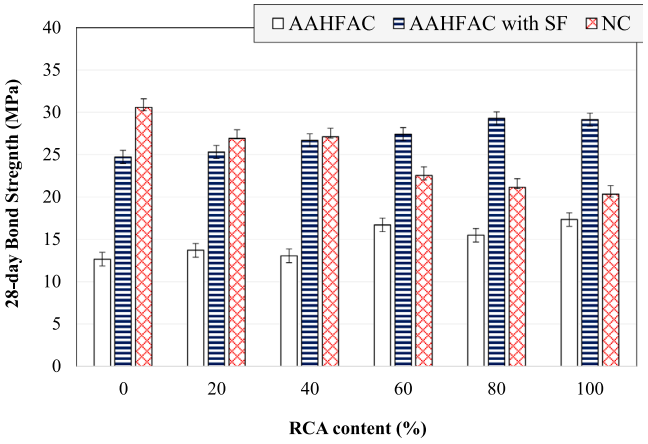

Fig. 11. Bond strength of AAHFAC, AAHFAC with SF, and NC under different RCA contents.

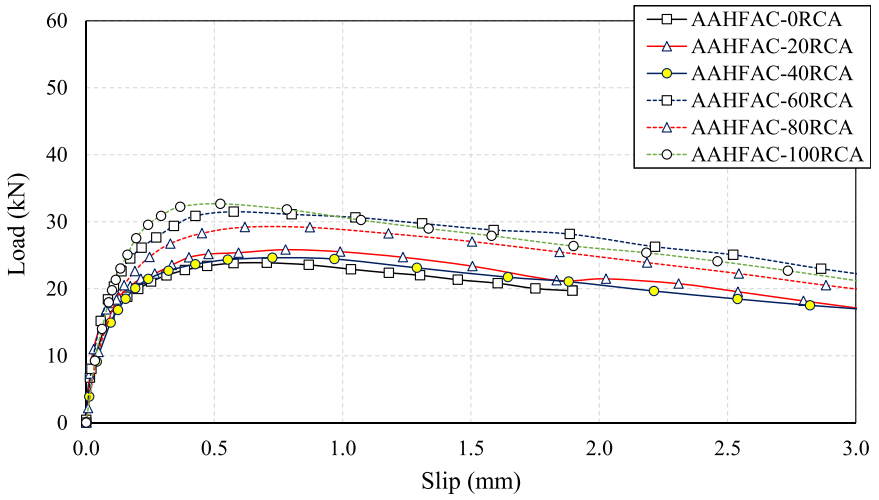

Fig. 12. Load-slip curves of AAHFAC under different RCA contents.

the same pattern. Both AAHFAC and AAHFAC with SF had increased load capacity as the RCA replacement increased (see Figs. 12–13). As explained previously, the addition of reaction products at the contact zone between AAB and RCA facilitated the development of their bond strength. While the load capacity of the NC mixes decreased as RCA replacement increased (see Fig. 14). These findings revealed that the bond resistance occurred in a similar way to the works of John Robert Prince and Singh [56] and Xiao and Falkner [57]. Recently, Xie and Zhao [58] presented a partial-interaction mechanics-based model to simulate the bond-slip response between steel bars and RAC, covering scenarios from a steel bar pulled out from RAC to the tension stiffening in reinforced RAC members. Similar models could be developed for AAHFAC and AAHFAC with SF but more experimental data are needed.

Fig. 15 shows the relationship between bond strength and compressive strength of concrete under different RCA contents. The logarithm function was used to display the relationship between the bond strength and compressive strength of all concrete containing RCA. This empirical equation has been successfully applied for normal concrete as described in ACI408R-03 [59]. An empirical equation with a high R^2 value of 0.962 and 0.929, respectively, could be utilized to express the bond strength of AAB and NC in relationship to the RCA content, as shown in Eqs. (2) and (3). Note, the constants in Eqs. (2) and (3) were determined by fitting curves to the results for RCA replacement levels of 0%, 20%, 40%, 60%, 80%, and 100%. Additionally, the bond strength models based on ACI408R-03 [59] and CEB-FIP [60] are provided with square root functions of concrete strength, as illustrated in Eqs. (4) and (5). It can be observed from Fig. 16 that the bond strength of the AAB and NC expressed as a function of $\sqrt{f_c'}/D$ was higher than those of normal concrete predicted by ACI408R-03 [59] and CEB-FIP [60]. The bond strength of AAB obtained from the present experiment was comparable to that of high strength concrete as determined by Orangun et al. [61] and Esfahani and Rangan [62], but was less than that of NC. Additionally, the bond strengths obtained in the present experiment were greater than those reported by Topark-Ngarm et al. [63] for high-calcium fly ash geopolymer concrete.

$$u_{AAB} = 0.532\left(\frac{\sqrt{f_c'}}{D}\right)^{2.24} \tag{2}$$

$$u_{NC} = 0.126\left(\frac{\sqrt{f_c'}}{D}\right)^{3.32} \tag{3}$$

ACI408R-03 [59] code:

$$u = 0.85\frac{\sqrt{f_c'}}{D} \tag{4}$$

CEB-FIP [60] code:

$$u = 2.0\frac{\sqrt{f_c'}}{D} \tag{5}$$

Where u is the ultimate bond strength (MPa), f_c' is the compressive strength (MPa), and D is the diameter of the deformed bar (cm).

The equivalent substrate stiffness (k_s) is an important parameter necessary in the design of the substrate-structure interaction members i.e., beam on foundation, stretchable electronics, and so on [64]. This equivalent substrate stiffness (k_s) can be calculated by the imposed displacement at an end point or free-end slip (l_{end}). ACI408R-03 [59] reported that the equivalent substrate stiffness (k_s) is called "friction force" among the surface of the bar. The conceptualization of the equivalent substrate stiffness (k_s) and bond force transfer mechanisms are shown in Fig. 16. Eq. (6) illustrates the relationship between the equivalent substrate stiffness and the end displacement of concrete pullout specimens with reinforcing bars. This equation stems from the concept of bar problem embedded in the elastic foundation as proposed by Limkatanyu et al. [65]. Tables 6–7 and Fig. 17 show

comparison of the equivalent substrate stiffnesses (k_s) of AAHFAC, AAHFAC with SF, and NC with various different RCA contents. It can be seen that the equivalent substrate stiffness (k_s) of AAHFAC and AAHFAC with SF tended to increase with increasing RCA substitution, except for AAHFAC-SF-0RCA and AAHFAC-SF-100RCA mixes. This is because the experimental results are low in slip. For the NC mixes, it is demonstrated that when RCA replacement increased, the equivalent substrate stiffness (k_s) appeared to decrease.

$$l_{end} = \frac{P\coth\left(\sqrt{k_s/E_sA_s}\,L\right)}{\sqrt{k_sE_sA_s}} \tag{6}$$

Where l_{end} is the imposed displacement at an end point (m), P is the imposed force at an end point (kN), k_s is the equivalent substrate stiffness (kN/m), E_s is the elastic modulus of reinforcing bars (GPa), A_s is the area of reinforcing bars (m^2), and L is the embedded length (m).

3.5. Life-cycle assessment

The life-cycle assessment (LCA) of AAHFAC, AAHFAC with SF, and NC at various RCA contents were evaluated. For the LCA

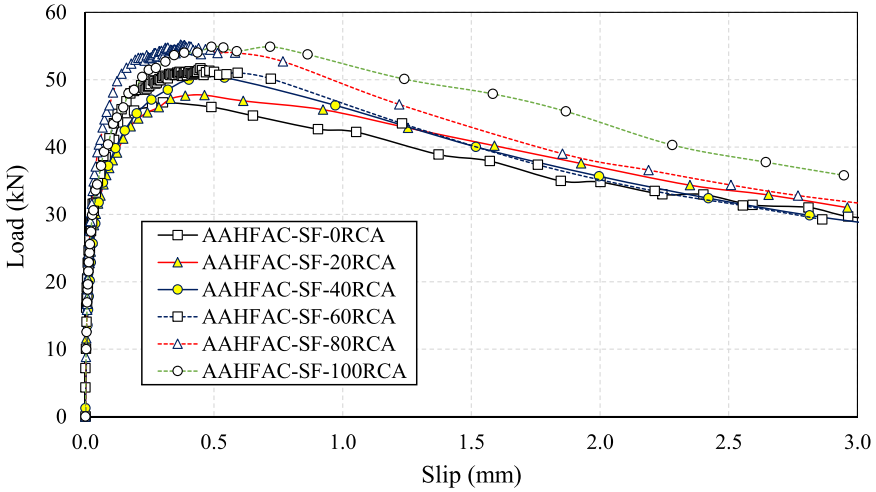

Fig. 13. Load-slip curves of AAHFAC incorporating SF under different RCA contents.

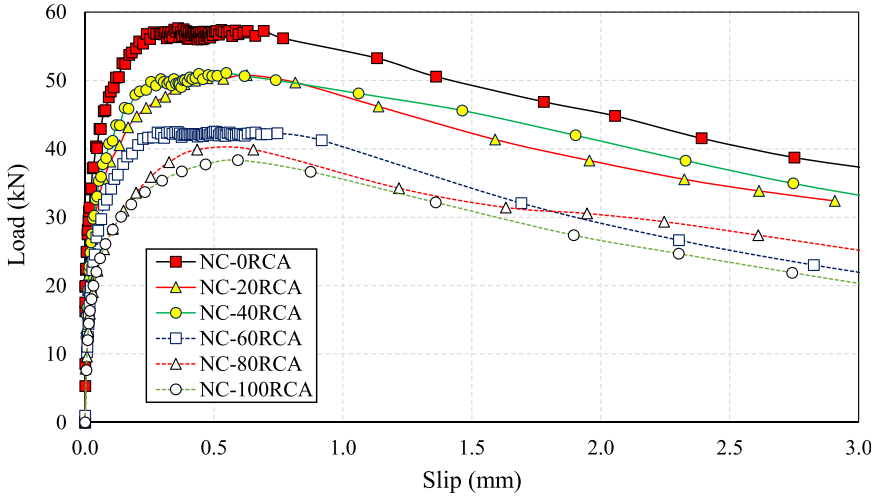

Fig. 14. Load-slip curves of NC under different RCA contents.

analysis, the unit of measurement is CO_2-e emitted (t CO_2-e/ton), as stated previously [11,66]. The emission factors in Table 8 are derived from the literature [67–71]. It is observed that HFA emits the lowest CO_2, whereas SS solution emits the most CO_2. Tables 9 and 10 illustrate the LCA calculations for AAHFAC, AAHFAC with SF, and NC at various RCA contents. The CO_2-e emitted value tended to decrease as the RCA replacement level increased for all types of concrete. A mixture containing 100%RCA seems to have the potential to reduce CO_2-e emissions by approximately 54% for AAB mixes and 31.5% for NC mixes. According to Tables 9–10, the AAHFAC-100RCA and AAHFAC-SF-100RCA mixes generated the lowest CO_2-e at 0.28197 and 0.28199 ton CO_2-e/ton, respectively. Additionally, the CO_2-e emission values for AAHFAC and AAHFAC with SF were clearly lower than the NC mixes. For instance, the CO_2-e emitted values were 0.41434, 0.41435, and 0.54085 ton CO_2-e/ton for AAHFAC, AAHFAC with SF, and NC, respectively. It can be concluded that incorporating RCA in AAB has a significant advantage, including improved strength development and a low carbon footprint.

4. Conclusion

From the results of the equivalent substrate stiffness and mechanical properties of sustainable alkali-activated concrete obtained from the study, the following conclusions can be drawn:

1) The use of RCA as a coarse aggregate in the AAHFAC and NC mixes decreased the setting times. The setting times of the AAHFAC with and without SF were shorter than that of NC mixes. The differences of reaction products in AAHFAC and NC were reasonable

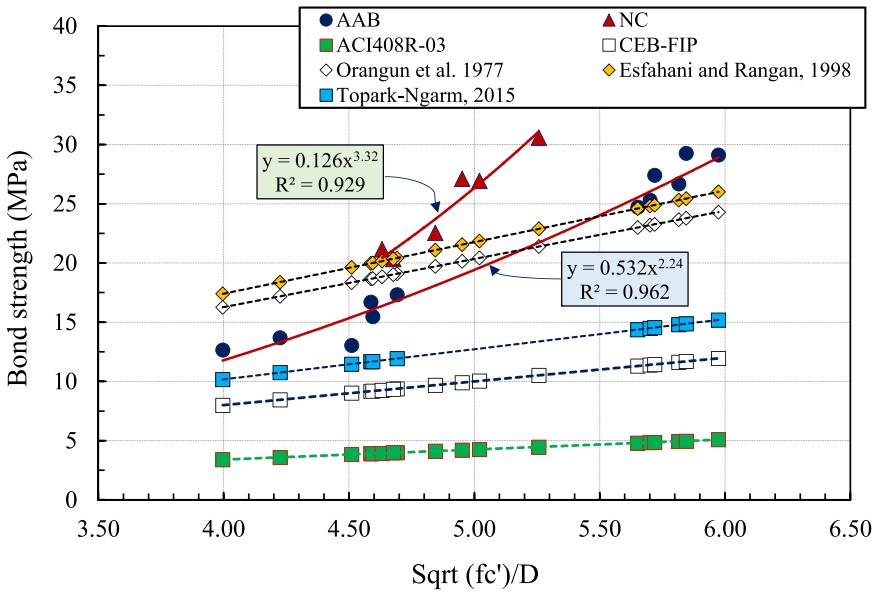

Fig. 15. Relationship between bond strength and compressive strength of concrete under different RCA contents.

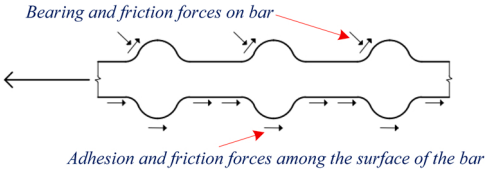

Fig. 16. Bond force transfer mechanisms [59].

Table 6
Equivalent substrate stiffness values of AAHFAC and AAHFAC with SF.

Mix No.	Mix symbol	Experimental					Numerical simulation	
		P (kN)	Slip (mm)	L (mm)	E_s (GPa)	A_s (mm^2)	k_s (MN/m)	Slip (mm)
1	AAHFAC-0RCA	23.87	0.70370	50	200	113.04	695.72	*0.7037*
2	AAHFAC-20RCA	25.83	0.77676	50	200	113.04	681.63	*0.7768*
3	AAHFAC-40RCA	24.62	0.72598	50	200	113.04	695.46	*0.7260*
4	AAHFAC-60RCA	31.49	0.57479	50	200	113.04	1141.36	*0.5748*
5	AAHFAC-80RCA	29.19	0.61882	50	200	113.04	977.17	*0.6188*
6	AAHFAC-100RCA	32.67	0.52286	50	200	113.04	1309.55	*0.5229*
7	AAHFAC-SF-0RCA	46.63	0.30155	50	200	113.04	3479.51	*0.3015*
8	AAHFAC-SF-20RCA	47.71	0.46271	50	200	113.04	2229.05	*0.4627*
9	AAHFAC-SF-40RCA	50.31	0.54045	50	200	113.04	1996.83	*0.5404*
10	AAHFAC-SF-60RCA	51.69	0.44720	50	200	113.04	2522.75	*0.4472*
11	AAHFAC-SF-80RCA	55.19	0.37027	50	200	113.04	3339.52	*0.3703*
12	AAHFAC-SF-100RCA	54.90	0.71809	50	200	113.04	1619.23	*0.7181*

Table 7
Equivalent substrate stiffness values of NC.

Mix No.	Mix symbol	Experimental					Numerical simulation	
		P (kN)	Slip (mm)	L (mm)	E_s (GPa)	A_s (mm^2)	k_s (MN/m)	Slip (mm)
1	NC-0RCA	57.65	0.36071	50	200	113.04	*3611.38*	*0.3607*
2	NC-20RCA	50.77	0.62717	50	200	113.04	*1720.28*	*0.6272*
3	NC-40RCA	51.11	0.54737	50	200	113.04	*2003.27*	*0.5474*
4	NC-60RCA	42.51	0.50271	50	200	113.04	*1802.34*	*0.5027*
5	NC-80RCA	39.89	0.65317	50	200	113.04	*1278.52*	*0.6532*
6	NC-100RCA	38.33	0.59297	50	200	113.04	*1356.97*	*0.5930*

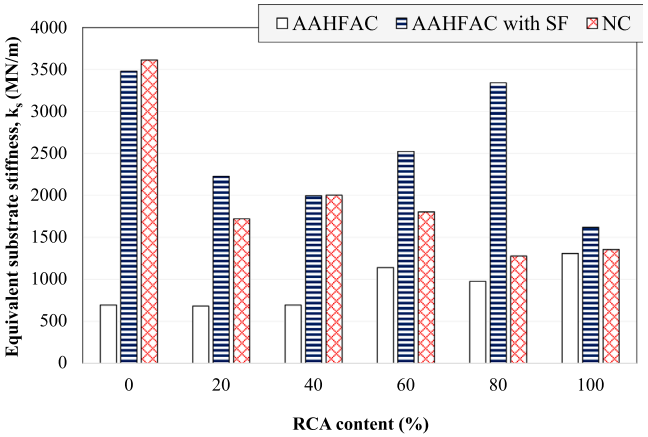

Fig. 17. Equivalent substrate stiffness of concrete under different RCA contents.

Table 8
The emission factors of tested materials [67–71].

Materials	Emission factor (t CO_2-e/ton)
Portland cement, PC (kg)	0.8200
River sand, RS (kg)	0.0139
Natural coarse aggregate, NCA (kg)	0.4300
Recycled concrete aggregate, RCA (kg)	0.1478
High-calcium fly ash, FA (kg)	0.0070
Silica Fume, SF (kg)	0.0100
Sodium hydroxide, SH (kg)	0.7000
Sodium silicate, SS (kg)	1.5140

for this case. Moreover, using RCA in AAHFAC incorporating SF showed a very fast setting compared to the AAHFAC, due to additional the reaction products within the matrix.

2) The increase in the RCA replacement level showed a positive effect on the strength development of both AAHFAC and AAHFAC incorporating SF; however, there seemed to provide a negative effect on NC mixes. The existence of hydration products on surface RCA could react with SiO_2 and Al_2O_3 from the precursors and hence became a more reaction products at contact zone between RCA and AAB.
3) The elastic modulus and strain capacity of the AAHFAC and AAHFAC incorporating SF mixes tended to increase with increasing amount of RCA replacement. The reaction between hydration products on surface RCA and SiO_2 and/or Al_2O_3 from the precursors provided a high bonding at the interfacial transition zone in concrete. Likewise, the strain capacity of the NC mixes tended to increase as the RCA replacement level increased; however, its elastic modulus decreased with increasing RCA content.
4) The Poisson's ratio values of the AAHFAC and AAHFAC incorporating SF were higher than that of the NC mixes. They were corresponded to the Poisson's ratio values of high-strength concrete.
5) Bond strengths of AAHFAC and AAHFAC with SF increased as RCA replacement was increased; nevertheless, bond strengths declined at NC mixes. The addition of reaction products at the AAB and RCA contact zone assisted in the improvement of their bond strength.
6) Both AAHFAC and AAHFAC with SF and RCA are viable options for sustainable concrete. They provide excellent strength development and bond strength between deformed bars and concrete with generating low CO_2.

Table 9
LCA analysis of AAHFAC and AAHFAC with SF from this study.

Mix symbol	HFA (kg)	CO_2-e/t from HFA	SF (kg)	CO_2-e/t from SF	RS (kg)	CO_2-e/t from RS	NCA (kg)	CO_2-e/t from NCA	RCA (kg)	CO_2-e/t from RCA	SH (kg)	CO_2-e/t from SH	SS (kg)	CO_2-e/t from SS	Total CO_2-e/t
AAHFAC-0RCA	470	0.0033	–	–	539	0.0075	1165	0.5010		0.0000	117.5	0.0247	117.5	0.0765	0.61290
AAHFAC-20RCA	470	0.0033	–	–	508	0.0071	932	0.4008	233	0.0344	117.5	0.0247	117.5	0.0765	0.54672
AAHFAC-40RCA	470	0.0033	–	–	477	0.0066	699	0.3006	466	0.0689	117.5	0.0247	117.5	0.0765	0.48053
AAHFAC-60RCA	470	0.0033	–	–	445	0.0062	466	0.2004	699	0.1033	117.5	0.0247	117.5	0.0765	0.41434
AAHFAC-80RCA	470	0.0033	–	–	414	0.0058	233	0.1002	932	0.1377	117.5	0.0247	117.5	0.0765	0.34815
AAHFAC-100RCA	470	0.0033	–	–	383	0.0053		0.0000	1165	0.1722	117.5	0.0247	117.5	0.0765	0.28197
AAHFAC-SF-0RCA	470	0.0033	47	0.0005	530	0.0074	1165	0.5010	–	–	117.5	0.0247	117.5	0.0765	0.61292
AAHFAC-SF-20RCA	423	0.0030	47	0.0005	498	0.0069	932	0.4008	233	0.0344	117.5	0.0247	117.5	0.0765	0.54672
AAHFAC-SF-40RCA	423	0.0030	47	0.0005	467	0.0065	699	0.3006	466	0.0689	117.5	0.0247	117.5	0.0765	0.48054
AAHFAC-SF-60RCA	423	0.0030	47	0.0005	436	0.0061	466	0.2004	699	0.1033	117.5	0.0247	117.5	0.0765	0.41435
AAHFAC-SF-80RCA	423	0.0030	47	0.0005	405	0.0056	233	0.1002	932	0.1377	117.5	0.0247	117.5	0.0765	0.34817
AAHFAC-SF-100RCA	423	0.0030	47	0.0005	374	0.0052	–	–	1165	0.1722	117.5	0.0247	117.5	0.0765	0.28199

Table 10
LCA analysis of NC from this study.

Mix symbol	PC (kg)	CO_2-e/t from PC	RS (kg)	CO_2-e/t from RS	NCA (kg)	CO_2-e/t from NCA	RCA (kg)	CO_2-e/t from RCA	Total CO_2-e/t
NC-0RCA	410	0.3362	905	0.0126	740	0.3182	–	–	0.66698
NC-20RCA	410	0.3362	885	0.0123	592	0.2546	148	0.0219	0.62494
NC-40RCA	410	0.3362	865	0.0120	444	0.1909	296	0.0437	0.58289
NC-60RCA	410	0.3362	845	0.0117	296	0.1273	444	0.0656	0.54085
NC-80RCA	410	0.3362	826	0.0115	148	0.0636	592	0.0875	0.49882
NC-100RCA	410	0.3362	806	0.0112	–	–	740	0.1094	0.45678

Declaration of Competing Interest

The authors declare that they have no known competing financial interests or personal relationships that could have appeared to influence the work reported in this paper.

Acknowledgments

This research has received funding support from the NSRF via the Program Management Unit for Human Resources & Institutional Development, Research and Innovation [grant number B05F630106]; and Unit of Excellence for Innovation in Infrastructures and Advanced Construction Management, University of Phayao, Grant no. FF64-UoE001. The authors also would like to acknowledge the support of the Department of Civil Engineering, Faculty of Engineering and Technology, Rajamangala University of Technology Isan, Thailand.

References

[1] G. Habert, J.B. d'Espinose de Lacaillerie, N. Roussel, An environmental evaluation of geopolymer based concrete production: reviewing current research trends, J. Clean. Prod. 19 (11) (2011) 1229–1238.
[2] B.C. McLellan, R.P. Williams, J. Lay, A. van Riessen, G.D. Corder, Costs and carbon emissions for geopolymer pastes in comparison to ordinary portland cement, J. Clean. Prod. 19 (9–10) (2011) 1080–1090.
[3] S. Mesgari, A. Akbarnezhad, J.Z. Xiao, Recycled geopolymer aggregates as coarse aggregates for Portland cement concrete and geopolymer concrete: effects on mechanical properties, Constr. Build. Mater. 236 (2020), 117571.
[4] J. Suebsuk, S. Horpibulsuk, A. Suksan, C. Suksiripattanapong, T. Phoo-ngernkham, A. Arulrajah, Strength prediction of cement-stabilised reclaimed asphalt pavement and lateritic soil blends, Int. J. Pavement Eng. 20 (3) (2019) 332–338.
[5] A. Wongsa, A. Siriwattanakarn, P. Nuaklong, V. Sata, P. Sukontasukkul, P. Chindaprasirt, Use of recycled aggregates in pressed fly ash geopolymer concrete, Environ. Prog. Sustain. Energy 39 (2) (2020), e13327.
[6] J. Nobre, M. Bravo, J. de Brito, G. Duarte, Durability performance of dry-mix shotcrete produced with coarse recycled concrete aggregates, J. Build. Eng. 29 (2020), 101135.
[7] T. Xie, G. Yang, X. Zhao, J. Xu, C. Fang, A unified model for predicting the compressive strength of recycled aggregate concrete containing supplementary cementitious materials, J. Clean. Prod. 251 (2020), 119752.
[8] S. Arabiyat, M. Abdel Jaber, H. Katkhuda, N. Shatarat, Influence of using two types of recycled aggregates on shear behavior of concrete beams, Constr. Build. Mater. 279 (2021), 122475.
[9] P. Nath, P.K. Sarker, Use of OPC to improve setting and early strength properties of low calcium fly ash geopolymer concrete cured at room temperature, Cem. Concr. Compos. 55 (0) (2015) 205–214.
[10] T. Phoo-ngernkham, C. Phiangphimai, N. Damrongwiriyanupap, S. Hanjitsuwan, J. Thumrongvut, P. Chindaprasirt, A mix design procedure for alkali-activated high-calcium fly ash concrete cured at ambient temperature, Adv. Mater. Sci. Eng. 2018 (2018) 13.
[11] T. Phoo-ngernkham, C. Phiangphimai, D. Intarabut, S. Hanjitsuwan, N. Damrongwiriyanupap, L.Y. Li, et al., Low cost and sustainable repair material made from alkali-activated high-calcium fly ash with calcium carbide residue, Constr. Build. Mater. 247 (2020), 118543.
[12] S.S. Rahman, M.J. Khattak, Roller compacted geopolymer concrete using recycled concrete aggregate, Constr. Build. Mater. 283 (2021), 122624.
[13] H.M. Abdalla, B.L. Karihaloo, Determination of size-independent specific fracture energy of concrete from three-point bend and wedge splitting tests, Mag. Concr. Res. 55 (2) (2003) 133–141.
[14] A.M. Aguirre-Guerrero, R.A. Robayo-Salazar, R.M. de Gutiérrez, A novel geopolymer application: coatings to protect reinforced concrete against corrosion, Appl. Clay Sci. 135 (2017) 437–446.
[15] P. Duan, C. Yan, W. Luo, A novel waterproof, fast setting and high early strength repair material derived from metakaolin geopolymer, Constr. Build. Mater. 124 (2016) 69–73.
[16] S.C. Yaragal, B. Chetan Kumar, C. Jitin, Durability studies on ferrochrome slag as coarse aggregate in sustainable alkali activated slag/fly ash based concretes, Sustain. Mater. Technol. 23 (2020), e00137.
[17] F. Pacheco-Torgal, J. Castro-Gomes, S. Jalali, Alkali-activated binders: a review. Part 1. Historical background, terminology, reaction mechanisms and hydration products, Constr. Build. Mater. 22 (7) (2008) 1305–1314.
[18] N. Damrongwiriyanupap, A. Wachum, K. Khansamrit, S. Detphan, S. Hanjitsuwan, T. Phoo-ngernkham, et al., Improvement of recycled concrete aggregate using alkali-activated binder treatment, Mater. Struct. 55 (1) (2021) 11.
[19] C. Detphan, P. Kaeorawang, B. Injorhor, K. Chompoovong, S. Hanjitsuwan, T. Phoo-ngernkham, et al., Improving drying shrinkage and strength development of alkali-activated high-calcium fly ash using commercial-grade calcium sulfate as expansive additive, Eng. Appl. Sci. Res. 49 (1) (2022) 58–64.
[20] T. Xie, P. Visintin, X. Zhao, R. Gravina, Mix design and mechanical properties of geopolymer and alkali activated concrete: review of the state-of-the-art and the development of a new unified approach, Constr. Build. Mater. 256 (2020), 119380.
[21] T. Xie, T. Ozbakkaloglu, Influence of coal ash properties on compressive behaviour of FA- and BA-based GPC, Mag. Concr. Res. 67 (24) (2015) 1301–1314.
[22] P. Chindaprasirt, T. Phoo-ngernkham, S. Hanjitsuwan, S. Horpibulsuk, A. Poowancum, B. Injorhor, Effect of calcium-rich compounds on setting time and strength development of alkali-activated fly ash cured at ambient temperature, Case Stud. Construct. Mater. 9 (2018) 1–9.
[23] T. Phoo-ngernkham, P. Chindaprasirt, V. Sata, S. Hanjitsuwan, S. Hatanaka, The effect of adding nano-SiO_2 and nano-Al_2O_3 on properties of high calcium fly ash geopolymer cured at ambient temperature, Mater. Des. 55 (0) (2014) 58–65.
[24] T. Phoo-ngernkham, S. Hanjitsuwan, L.Y. Li, N. Damrongwiriyanupap, P. Chindaprasirt, Adhesion characterization of Portland cement concrete and alkali-activated binders under different types of calcium promoters, Adv. Cem. Res. 31 (2) (2019) 69–79.
[25] T. Phoo-ngernkham, V. Sata, S. Hanjitsuwan, C. Ridtirud, S. Hatanaka, P. Chindaprasirt, High calcium fly ash geopolymer mortar containing Portland cement for use as repair material, Constr. Build. Mater. 98 (2015) 482–488.
[26] V. Sata, A. Wongsa, P. Chindaprasirt, Properties of pervious geopolymer concrete using recycled aggregates, Constr. Build. Mater. 42 (0) (2013) 33–39.
[27] P. Nuaklong, V. Sata, P. Chindaprasirt, Properties of metakaolin-high calcium fly ash geopolymer concrete containing recycled aggregate from crushed concrete specimens, Constr. Build. Mater. 161 (2018) 365–373.
[28] K. Pasupathy, S. Ramakrishnan, J. Sanjayan, Influence of recycled concrete aggregate on the foam stability of aerated geopolymer concrete, Constr. Build. Mater. 271 (2021), 121850.
[29] J. Wang, J. Xie, C. Wang, J. Zhao, F. Liu, C. Fang, Study on the optimum initial curing condition for fly ash and GGBS based geopolymer recycled aggregate concrete, Constr. Build. Mater. 247 (2020), 118540.
[30] Jianhe Xie, Wei Chen, Junjie Wang, Chi Fang, Bingxue Zhang, Feng Liu, Coupling effects of recycled aggregate and GGBS/metakaolin on physicochemical properties of geopolymer concrete, Constr. Build. Mater. 226 (2019) 345–359.
[31] ACI 211.1-91, Standard practice for selecting proportions for normal, heavyweight, and mass concrete, Am. Concr. Inst. (1991) 1–38.
[32] ASTM C403/C403M-16, Standard test method for time of setting of concrete mixtures by penetration resistance, Annu. Book ASTM Stand. 04.02 (2016).

[33] ASTM C469/C469M-14e1, Standard test method for static modulus of elasticity and poisson's ratio of concrete in compression, Annu. Book ASTM Stand. 02.01. (2014).
[34] ASTM C234-91, Standard test method for comparing concretes on the basis of the bond developed with reinforcing steel, Annu. Book ASTM Stand. (1991) 1–5 (Philadelphia).
[35] T.C. Rilem, RC 6 bond test for reinforcement steel. 2. Pull-out test, 1983. RILEM technical recommendations for the testing and use of constructions, Materials (1994) 218–220.
[36] A. Castel, S.J. Foster, Bond strength between blended slag and Class F fly ash geopolymer concrete with steel reinforcement, Cem. Concr. Res. 72 (2015) 48–53.
[37] P. Chindaprasirt, P. De Silva, K. Sagoe-Crenstil, S. Hanjitsuwan, Effect of SiO_2 and Al_2O_3 on the setting and hardening of high calcium fly ash-based geopolymer systems, J. Mater. Sci. 47 (12) (2012) 4876–4883.
[38] S. Hanjitsuwan, B. Injorhor, T. Phoo-ngernkham, N. Damrongwiriyanupap, L.Y. Li, P. Sukontasukkul, et al., Drying shrinkage, strength and microstructure of alkali-activated high-calcium fly ash using FGD-gypsum and dolomite as expansive additive, Cem. Concr. Compos. 114 (2020), 103760.
[39] P. Sukontasukkul, P. Chindaprasirt, P. Pongsopha, T. Phoo-Ngernkham, W. Tangchirapat, N. Banthia, Effect of fly ash/silica fume ratio and curing condition on mechanical properties of fiber-reinforced geopolymer, J. Sustain. Cem. -Based Mater. (2020) 1–15.
[40] P. Rattanachu, W. Tangchirapat, C. Jaturapitakkul, Water permeability and sulfate resistance of eco-friendly high-strength concrete composed of ground bagasse ash and recycled concrete aggregate, J. Mater. Civ. Eng. 31 (6) (2019), 04019093.
[41] N. Li, C. Shi, Q. Wang, Z. Zhang, Z. Ou, Composition design and performance of alkali-activated cements, Mater. Struct. 50 (3) (2017) 178.
[42] V. Sata, A. Wongsa, P. Chindaprasirt, Properties of pervious geopolymer concrete using recycled aggregates, Constr. Build. Mater. 42 (2013) 33–39.
[43] W. Kroehong, T. Sinsiri, C. Jaturapitakkul, P. Chindaprasirt, Effect of palm oil fuel ash fineness on the microstructure of blended cement paste, Constr. Build. Mater. 25 (11) (2011) 4095–4104.
[44] T. Phoo-ngernkham, P. Chindaprasirt, V. Sata, S. Pangdaeng, T. Sinsiri, Properteis of high calcium fly ash geopolymer pastes containing Portland cement as additive, Int. J. Miner., Metall. Mater. 20 (2) (2013) 214–220.
[45] T. Sinsiri, T. Phoo-ngernkham, V. Sata, P. Chindaprasirt, The effects of replacement fly ash with diatomite in geopolymer mortar, Comput. Concr. 9 (6) (2012) 427–437.
[46] Z. Wang, J. Zuo, X. Zhang, G. Jiang, L. Feng, Stress–strain behaviour of hybrid-fibre engineered cementitious composite in compression, Adv. Cem. Res. 32 (2) (2020) 53–65.
[47] ACI 318-14, Building code requirements for structural concrete (ACI 318-14) and commentary (318R-14), Am. Concr. Inst. (2014) 49–56.
[48] M. Sofi, J.S.J. van Deventer, P.A. Mendis, G.C. Lukey, Engineering properties of inorganic polymer concretes (IPCs), Cem. Concr. Res. 37 (2) (2007) 251–257.
[49] W. Tangchirapat, S. Khamklai, C. Jaturapitakkul, Use of ground palm oil fuel ash to improve strength, sulfate resistance, and water permeability of concrete containing high amount of recycled concrete aggregates, Mater. Des. 41 (2012) 150–157.
[50] P. Nath, P.K. Sarker, Flexural strength and elastic modulus of ambient-cured blended low-calcium fly ash geopolymer concrete, Constr. Build. Mater. 130 (Supplement C) (2017) 22–31.
[51] M. Shariq, J. Prasad, H. Abbas, Effect of GGBFS on age dependent static modulus of elasticity of concrete, Constr. Build. Mater. 41 (Supplement C) (2013) 411–418.
[52] M. Alhawat, A. Ashour, Bond strength between corroded steel and recycled aggregate concrete incorporating nano silica, Constr. Build. Mater. 237 (2020), 117441.
[53] F. Pacheco-Torgal, J.P. Castro-Gomes, S. Jalali, Adhesion characterization of tungsten mine waste geopolymeric binder. Influence of OPC concrete substrate surface treatment, Constr. Build. Mater. 22 (3) (2008) 154–161.
[54] P. Chindaprasirt, P. Sukontasukkul, A. Techaphatthanakon, S. Kongtun, C. Ruttanapun, D.Y. Yoo, et al., Effect of graphene oxide on single fiber pullout behavior, Constr. Build. Mater. 280 (2021), 122539.
[55] D.Y. Yoo, J. Je, H.J. Choi, P. Sukontasukkul, Influence of embedment length on the pullout behavior of steel fibers from ultra-high-performance concrete, Mater. Lett. 276 (2020), 128233.
[56] M. John Robert Prince, B. Singh, Bond behaviour of deformed steel bars embedded in recycled aggregate concrete, Constr. Build. Mater. 49 (0) (2013) 852–862.
[57] J. Xiao, H. Falkner, Bond behaviour between recycled aggregate concrete and steel rebars, Constr. Build. Mater. 21 (2) (2007) 395–401.
[58] T. Xie, X. Zhao, Can a local bond test truly reflect impact of recycled aggregate on the bond between deformed steel bars and recycled aggregate concrete? – a critical assessment and development of a generic model, Eng. Struct. 244 (2021), 112826.
[59] ACI 408R-03, Bond and Development of Straight Reinforcing Bars in Tension, Am. Concr. Inst. (2003) 1–49.
[60] CEB-FIP, CEB-FIP model code for concrete structures, Bull. Eur. Comm. Concr. (1990) 82–115.
[61] C.O. Orangun, J.O. Jirsa, J.E. Breen, A reevaluation of test data on development length and splices, Acids Struct. J. 74 (3) (1977) 114–122.
[62] M.R. Esfahani, B.V. Rangan, Bond between normal strength and high-strength concrete (HSC) and reinforcing bars in splices in beams, Acids Struct. J. 95 (3) (1988) 272–280.
[63] P. Topark-Ngarm, P. Chindaprasirt, V. Sata, Setting time, strength, and bond of high-calcium fly ash geopolymer concrete, J. Mater. Civ. Eng. 27 (7) (2015), 04014198.
[64] A. Hanif, G. Ghosh, M. Meeseepong, H. Haq Chouhdry, A. Bag, M.V. Chinnamani, et al., A composite microfiber for biodegradable stretchable electronics, Micromachines 12 (9) (2021) 1036.
[65] S. Limkatanyu, N. Damrongwiriyanupap, W. Prachasaree, W. Sae-Long, Modeling of axially loaded nanowires embedded in elastic substrate media with inclusion of nonlocal and surface effects, J. Nanomater. 2013 (2013), 635428.
[66] T. Phoo-ngernkham, S. Hanjitsuwan, C. Suksiripattanapong, J. Thumrongvut, J. Suebsuk, S. Sookasem, Flexural strength of notched concrete beam filled with alkali-activated binders under different types of alkali solutions, Constr. Build. Mater. 127 (2016) 673–678.
[67] F.G. Collins, Inclusion of carbonation during the life cycle of built and recycled concrete: influence on their carbon footprint, Int. J. Life Cycle Assess. 15 (6) (2010) 549–556.
[68] L.K. Turner, F.G. Collins, Carbon dioxide equivalent (CO_2-e) emissions: a comparison between geopolymer and OPC cement concrete, Constr. Build. Mater. 43 (0) (2013) 125–130.
[69] Y. Zhang, W. Luo, J. Wang, Y.S. Wang, Y. Xu, J. Xiao, A review of life cycle assessment of recycled aggregate concrete, Constr. Build. Mater. 209 (2019) 115–125.
[70] M.U. Hossain, C.S. Poon, I.M.C. Lo, J.C.P. Cheng, Comparative environmental evaluation of aggregate production from recycled waste materials and virgin sources by LCA, Resour. Conserv. Recycl. 109 (2016) 67–77.
[71] Z. Zimele, M. Sinka, A. Korjakins, D. Bajare, G. Sahmenko, Life cycle assessment of foam concrete production in Latvia, Environ. Clim. Technol. 23 (3) (2019) 70–84.